fluctuations per unit of frequency, $S = \langle(i^2)\rangle/\Delta f$; for stochastic partitioning at zero temperature, $S \propto eV_{dc}T_{SD}(1 - T_{SD})$ (ref. 13). Introducing a phenomenological parameter k that accounts for decoherence in the interferometer with $T_1 = 1/2$ and $T_{SD} = 0.5 + k\sqrt{T_2(1 - T_2)}\cos\varphi$, we find that for complete phase averaging or for a complete decoherence $T_{SD} = 0.5$, namely, a constant. On the other hand, shot noise in D1 is $S_{D1} \propto T_{SD1}(1 - T_{SD1}) = 1/4 - k^2T_2(1 - T_2)\cos^2\varphi$, with $S_{D1} = $ const. for $k = 0$, but $S_{D1} = 1/4 - k^2T_2(1 - T_2)/2$ for complete phase averaging (resulting from an integration of $\cos^2\varphi$ in the range $\varphi = 0\ldots\ldots2\pi$). Hence, noise is expected to exhibit a parabolic dependence on T_2 in a coherent system. Shot noise was measured[12,13] with a relatively large V_{dc} applied at S so that interference signal was quenched (negligible visibility). The dependence of S on T_2, shown in Fig. 4, followed the above expression with $k \approx 0.9$, proving that phase averaging is indeed dominant while decoherence is negligibly small.

A single-particle model (that is, a non-interacting model) would lead to the following dependences of the visibility on energy: for $V = 0$ and finite T, $\nu \propto \beta T/\sinh(\beta T)$, with β a constant; for finite V but $T = 0$, $\nu \propto \sin[(e/2\pi)V]/[(e/2\pi)V]$, while the differential visibility at $T = 0$ is expected to be voltage independent. Because the experimental results contradict these predictions, we propose (with no proof yet) two possible reasons for the dephasing. One might be low-frequency noise (of, say, the $1/f$ type due to moving impurities), which might be induced by a higher current, leading to fluctuation in the area and consequently, phase smearing. The other could be related to the self-consistent potential contour at the edge. As it depends on the local density of the electrons in the edge state[14], fluctuation in the density due to partitioning are expected to lead to fluctuation in the AB area enclosed by the two paths and hence to phase randomization. For example, for $B \approx 5.5$ T, a shift of the edge of only 1–2 Å suffices to add one flux quantum into the enclosed area.

We believe that this electron interferometer might prove useful in future work on the interference of electrons. One possible area of research is the coherence and phase of fractionally charged quasiparticles in the fractional QHE regime[15]. □

Received 1 October 2002; accepted 12 February 2003; doi:10.1038/nature01503.

1. Yacoby, A., Heiblum, M., Umansky, V., Shtrikman, H. & Mahalu, D. Unexpected periodicity in an electronic double slit interference experiment. *Phys. Rev. Lett.* **73,** 3149–3152 (1994).
2. Yacoby, A., Heiblum, M., Mahalu, D. & Shtrikman, H. Coherency and phase sensitive measurements in a quantum dot. *Phys. Rev. Lett.* **74,** 4047–4050 (1994).
3. Schuster, R. *et al.* Phase measurement in a quantum dot via a double-slit interference measurement. *Nature* **385,** 417–420 (1997).
4. Ji, Y., Heiblum, M., Sprinzak, D., Mahalu, D. & Shtrikman, H. Phase evolution in a Kondo-correlated system. *Science* **290,** 779–783 (2000).
5. Buks, E., Schuster, R., Heiblum, M., Mahalu, D. & Shtrikman, H. Dephasing in electron interference by a 'which-path' detector. *Nature* **391,** 871–820 (1998).
6. van der Viel, W. G. *et al.* The Kondo effect at unitary limit. *Science* **289,** 2105–2108 (2000).
7. Buttiker, M. Four terminal phase coherent conductance. *Phys. Rev. Lett.* **57,** 1761–1764 (1986).
8. Prange, R. E. & Girvin, S. M. (eds) *The Quantum Hall Effect* (Springer, New York, 1987).
9. Born, M. & Wolf, E. *Principles of Optics* 348–352, 7th edn (Cambridge Univ. Press, Cambridge, UK, 1999).
10. Aharonov, Y. & Bohm, D. Significance of electromagnetic potentials in the quantum theory. *Phys. Rev.* **115,** 485–491 (1959).
11. Aronov, A. G. & Sharvin, Yu. V. Magnetic flux effects in disordered conductors. *Rev. Mod. Phys.* **59,** 755–779 (1987).
12. de-Picciotto, R. *et al.* Direct observation of a fractional charge. *Nature* **389,** 162–165 (1997).
13. Reznikov, M. *et al.* Quantum shot noise. *Superlattice Microstruct.* **23,** 901–915 (1998).
14. Chklovskii, D. B., Shklovskii, B. I. & Glazman, L. I. Electrostatics of edge channels. *Phys. Rev. B* **46,** 4026–4034 (1992).
15. Kane, C. L. Telegraph noise and fractional statistics in the quantum Hall effect. Preprint cond-mat/0210621 at ⟨http://xxx.lanl.gov⟩ (2002).

Acknowledgements We thank Y. Levinson for clarifying the issue of phase averaging, and C. Kane for comments on the manuscript. The work was partly supported by the MINERVA Foundation, the Israeli Academy of Science, the German Israeli Project Cooperation (DIP), the German Israeli Foundation (GIF), and the EU QUACS network.

Competing interests statement The authors declare that they have no competing financial interests.

Correspondence and requests for materials should be addressed to M.H. (e-mail: heiblum@wisemail.weizmann.ac.il).

African vegetation controlled by tropical sea surface temperatures in the mid-Pleistocene period

Enno Schefuß*, Stefan Schouten, J. H. Fred Jansen & Jaap S. Sinninghe Damsté

Royal Netherlands Institute for Sea Research (NIOZ), PO Box 59, 1790 AB Den Burg, The Netherlands

The dominant forcing factors for past large-scale changes in vegetation are widely debated. Changes in the distribution of C_4 plants—adapted to warm, dry conditions and low atmospheric CO_2 concentrations[1]—have been attributed to marked changes in environmental conditions, but the relative impacts of changes in aridity, temperature[2,3] and CO_2 concentration[4,5] are not well understood. Here, we present a record of African C_4 plant abundance between 1.2 and 0.45 million years ago, derived from compound-specific carbon isotope analyses of wind-transported terrigenous plant waxes. We find that large-scale changes in African vegetation are linked closely to sea surface temperatures in the tropical Atlantic Ocean. We conclude that, in the mid-Pleistocene, changes in atmospheric moisture content—driven by tropical sea surface temperature changes and the strength of the African monsoon—controlled aridity on the African continent, and hence large-scale vegetation changes.

Two main carbon fixation pathways of higher plant photosynthesis, the Calvin–Benson (C_3) and the Hatch–Slack (C_4) cycles, occur in natural ecosystems[6]. Nearly all trees, cold-season grasses and sedges use the C_3 pathway, whereas C_4 photosynthesis is found in warm-season grasses and sedges[7]. Thus, C_4 plants are found predominantly in tropical savannahs, temperate grasslands and semideserts[7]. Most African grasslands are dominated currently by C_4 plant vegetation[1]. C_4 plants use a CO_2-concentrating mechanism, thereby outcompeting C_3 plants at low atmospheric p_{CO_2} (ref. 8) and causing them to be isotopically enriched in ^{13}C (ref. 4). At high p_{CO_2}, however, C_3 plants will outcompete C_4 plants owing to the higher energy need of C_4 plants during photosynthesis[8]. The crossover between C_3 and C_4 plants depends also on the daytime growing-season temperature, with higher temperatures favouring C_4 plants[7,8]. Other factors, however, may also affect the occurrence of C_3 and C_4 plants. Where precipitation and nutrient availability permit trees to grow, C_3 trees will outcompete C_4 grasses, such as in the tropical forests[1]. The significance of the climatic factors determining the large-scale C_4 plant abundance is still not well understood, but insights can be gained from the analysis of past vegetation changes.

Long-chain, odd-numbered C_{25} to C_{35} *n*-alkanes are major lipid constituents of the epicuticular wax layer of terrestrial plants[9]. These plant waxes are easily removed from the leaf surface by rain or wind, especially by sandblasting during dust storms. They are, therefore, common organic components of eolian dust[10]. In surface sediments of the eastern South Atlantic, the plant wax *n*-alkanes exhibit a moderate to high odd versus even carbon-number predominance (carbon preference index (CPI) of 2.3–6.4), and thus predominantly represent leaf waxes of terrestrial higher plants[9]. Their plume-like distribution in surface sediments (Fig. 1a) indicates that they are primarily transported by southeasterly winds from the dry areas in southern Africa, the Kalahari savannah and Namib Desert. The discharge of the Congo River is apparently of minor importance for the supply of *n*-alkane leaf waxes. During the austral winter (June to August) the strong Southern Hemisphere trade winds transport

* Present address: Research Center Ocean Margins, University of Bremen, PO Box 330440, 28334 Bremen, Germany.

large amounts of dust northwestwards over the eastern South Atlantic (Fig. 2a). In the austral summer (December to February), during the southern African monsoon season, the trade winds are deflected landwards (Fig. 2b). We estimated the C_4-plant-derived percentage of leaf wax *n*-alkanes in surface sediments using the stable carbon isotopic composition ($\delta^{13}C$ in ‰ against PeeDee Belemnite (PDB)) of the predominating *n*-C_{31} alkane and a binary mixing equation, assuming $\delta^{13}C_4$ leaf wax lipids of −21.5‰ and $\delta^{13}C_3$ leaf wax lipids of −36.0‰ (ref. 11). The results (Fig. 1b) show that the $\delta^{13}C$ of leaf wax *n*-alkanes in the surface sediments of the eastern South Atlantic mainly reflect the contemporary vegetation zones on the adjacent continent (Fig. 2). This finding is supported by investigations of atmospheric dusts collected off the African coast[10]. The atmospheric plant wax lipids show a C_4 plant contribution of about 55% in dust from the southern African dry areas, whereas off the tropical rainforest regions the C_4 plant fraction is 30–40% (ref. 10).

On the basis of these insights into the present-day system, we reconstructed the mid-Pleistocene African C_3 to C_4 plant vegetation changes with a plant wax $\delta^{13}C$ record from Ocean Drilling Program (ODP) Site 1077 (10° 26.2′ E, 5° 10.8′ S, 2,382 m water depth) in the eastern tropical Atlantic Angola Basin (Fig. 1). This site is located at the northern edge of the modern Southern Hemisphere dust plume during the austral winter (Fig. 2a) and is thus sensitive to changes in its strength and position. It is, therefore, an ideal recorder of the southern African vegetation signal transported with plant wax lipids in dust. This record was compared with an alkenone record obtained from the same sediment core, reflecting the sea surface temperature (SST) (Fig. 3b), and the $\delta^{18}O$ record of benthic foraminifera at ODP Site 677 (ref. 12), reflecting the global ice volume (Fig. 3d). We investigated the period from 1.2 million years to 450 thousand years before present (kyr BP), including the mid-Pleistocene Transition (MPT), leading to the establishment of the 100-kyr rhythm of the Late Pleistocene ice ages around 650 kyr BP. Before the MPT, a 41-kyr cyclicity was prevalent. During the MPT, from about 920 to 650 kyr BP, the global ice volume variations increased in amplitude[13], which led to a substantial perturbation of the climate system, probably by re-adjustment of the enlarged Late Pleistocene ice sheets[14]. The global oceanic thermohaline circulation was severely weakened by a strong reduction of North Atlantic deepwater ventilation[15], probably causing the long-term surface water warming of the tropical Atlantic Ocean during the MPT, as revealed by our alkenone SST record (Fig. 3b).

The *n*-alkanes in the sediments of ODP Site 1077 are predominantly derived from higher-plant waxes (CPI = 2.1–5.3) supplied by the wind. The mid-Pleistocene record of the relative C_4 plant contribution shows large deviations (from 20% to 70%, Fig. 3a) from the present-day value (about 35%, Fig. 1b). To determine the dominant control on African C_4 plant abundance, cross-spectral analyses of the C_4 plant percentage, SST, global ice volume and *n*-alkane flux records with the ETP record—the summed variance of eccentricity, tilt (obliquity) and precession of the Earth's orbit—were performed.

Spectral analyses show that the *n*-alkane accumulation rates do not correlate with the C_4 plant changes in all orbital cycles (Table 1). So, an increased eolian flux of C_4 plant *n*-alkanes during times of elevated *n*-alkane accumulation rates cannot explain the C_4 plant record. The *n*-alkane fluxes (Fig. 3c) were generally low before 900 kyr BP, and increased after the growth of the global ice volume at around 900 kyr BP[14]. This suggests that the eolian transport of plant waxes responded to changes in the trade wind system. Conformably, an increase of the eolian terrigenous accumulation off northwest Africa around 900 kyr BP was attributed to the compression and strengthening of the atmospheric circulation cells[16] caused by the expansion of the mean global ice volume. Atmospheric trajectory calculations for this ocean area for the Last Glacial Maximum indicate higher wind speed, but a similar flow path[17]. Therefore, our C_4 plant record reflects predominantly the vegetation changes in southern Africa, and not a change in source area of the wax lipids.

The C_4 plant record correlates strongly with the SST development at ODP Site 1077 (Fig. 3b and Table 1). It co-varies in the precessional (23-kyr) cycle but acts in anti-phase in the obliquity (41-kyr) and eccentricity (100-kyr) cycles. In the precessional cycle, the maximum C_4 plant occurrence corresponds with the maximum SST. This is readily explained by the common low-latitude insolation forcing of the African monsoon and equatorial Atlantic upwelling[16,18,19], which are both mainly controlled by the strength of the precession[20]. Subtropical southern Africa receives its main precipitation during the austral summer monsoon[21] (Fig. 2b), whereas upwelling in the equatorial Atlantic is strongest during the austral winter[19,22,23] (Fig. 2a). The precessional variations in the summer insolation are in anti-phase between the hemispheres[20,21], inducing the strongest southern African monsoon when the northern African monsoon is weakest; that is, when equatorial upwelling

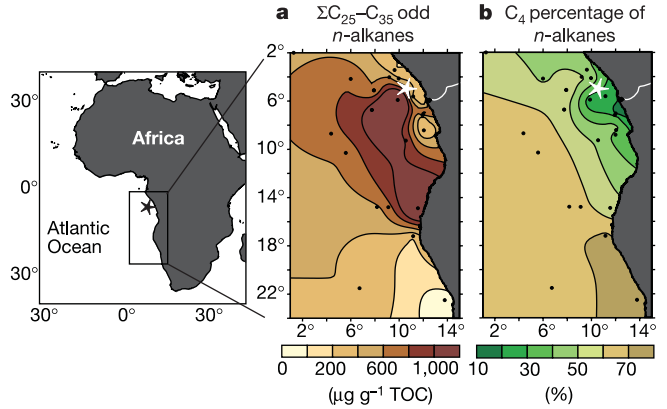

Figure 1 Modern distributions of plant wax concentrations and their vegetation signatures. **a**, **b**, Spatial distribution of the total organic carbon (TOC)-normalized concentrations of the C_{25} to C_{35} odd-numbered *n*-alkanes (**a**) and the C_4 plant percentage of the *n*-C_{31} alkane (**b**) in surface sediments. Isolines were calculated with the Surfer software program using the gridding method of kriging. Black dots are locations of surface samples taken during the RV *Tyro* cruise in 1989. The star indicates the location of ODP Site 1077.

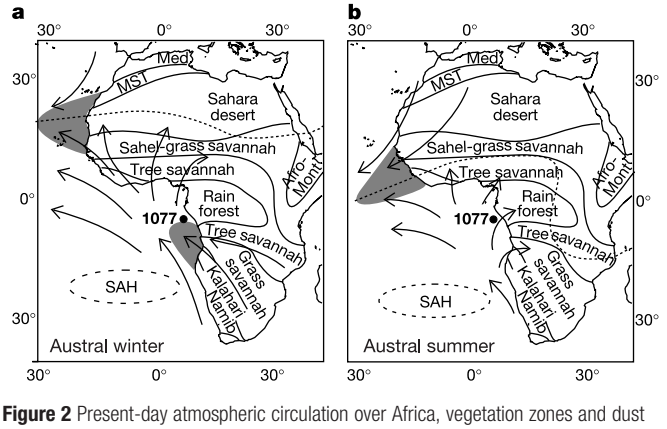

Figure 2 Present-day atmospheric circulation over Africa, vegetation zones and dust plumes. **a**, **b**, General pattern of present-day atmospheric circulation over Africa and the Southeast Atlantic Ocean in austral winter (**a**; June to August) and austral summer (**b**; December to February). SAH, South Atlantic high-pressure cell. The dotted line indicates the position of the intertropical convergence zone (ITCZ). Dust plumes are shaded. Areas in Africa indicate vegetation zones. The location of ODP site 1077 is indicated. Med, Mediterranean vegetation; MST, Mediterranean–Saharan transitional vegetation; Afro-Mont, Afro-montane vegetation zone.

is strongest. The most humid periods in southern Africa, favourable for C_3 plants, therefore coincide with periods of lowered tropical SST[19,21–23] in the precessional cycle. The precessional C_3 to C_4 plant variations in subtropical southern Africa are thus explained by changes in monsoonal precipitation, driven by the low-latitude insolation changes.

The enlarged mean global ice volume, reflected by the $\delta^{18}O$ of benthic foraminifera (Fig. 3d), increasingly affected the tropical vegetation[24] and the eolian transport (Fig. 3c) after 900 kyr BP. The 100-kyr rhythm of the Late Pleistocene ice ages is detected in all investigated records after about 650 kyr BP. The development of the global ice volume thus undoubtedly influenced the tropical environmental changes, following the frequency pattern set by the high latitudes. In the two longer orbital periods, eccentricity and obliquity, however, the changes in C_4 plant abundance significantly precede the variations of global ice volume and occur in phase with the tropical SST changes (Table 1). Moreover, the long-term C_4 plant record shows no correlation at all with the long-term global ice volume development (Fig. 3a, d), but it does resemble the long-term SST behaviour (Fig. 3b). The opposite phasing between maximum SST and maximum C_4 plant abundance in the two longer orbital cycles and in the long-term development (Table 1 and Fig. 3) excludes a direct temperature forcing of the observed C_3 to C_4 plant vegetation changes. Assuming that air temperatures over subtropical Africa changed in the same way as the tropical SST, lower temperatures in the growing season would have favoured C_3 plants and not C_4 plants, as is observed (Table 1). We, therefore, propose a common dominant control on large-scale C_3 to C_4 plant variations in southern Africa by continental aridity. In the precessional cycle, the aridity variations were driven by the strength of the monsoon, controlled by low-latitude insolation changes. Low-latitude insolation, however, contains neither an obliquity nor an eccentricity component[20]. This suggests that the tropical SST directly controlled the continental aridity in the longer orbital cycles and the long-term development, in line with recent modelling results[25] and modern climatological observations[26]. During the mid-Pleistocene, the tropical Atlantic SST (Fig. 3b) decreased by up to 5 °C during glacials, comparable to the Last Glacial Maximum[27]. The lowered SST reduced the tropical evaporation and the atmospheric moisture content, the main source for the African precipitation. This large-scale aridification must have been an important factor for the establishment and persistence of C_4 grasslands and even for the evolution of C_4 plants[28]. Enhanced aridity will also have increased the frequency of natural fires, deemed to be an important factor for increasing relative C_4 grass expansion in tropical savannahs[28]. These findings do not necessarily imply an independent behaviour of the C_4 plant abundance from the changes in global ice volume. The high-latitude climate signal manifests itself through its impact on the equatorial Atlantic SST variations[19,27] on the African vegetation changes.

Over the past 420 kyr, the ice-core records of atmospheric p_{CO_2} correlate strongly with ice volume records[29]. The phase differences between the C_4 plant abundance and the global ice volume record (Table 1) and especially their non-uniform long-term developments indicate, however, that large-scale C_3 to C_4 vegetation changes were not primarily controlled by atmospheric p_{CO_2} variations. This conclusion is supported by a reconstruction of p_{CO_2} for the Miocene, when C_4 grasses had widely expanded[7] without an accompanying decrease in atmospheric CO_2 concentrations[2]. Moreover, a low atmospheric p_{CO_2} alone is unable to trigger C_4 plant expansions, and aridity drives C_3 to C_4 plant abundance changes on a regional scale[3]. Our results indicate that aridity is the dominant climatic control of C_4 plant abundance on a large, continental scale and at various timescales. The variations in Pleistocene African vegetation were primarily forced by changes in the strength of the monsoon and changes in the atmospheric moisture balance directly controlled by the tropical SST. Low-latitude sea-surface conditions

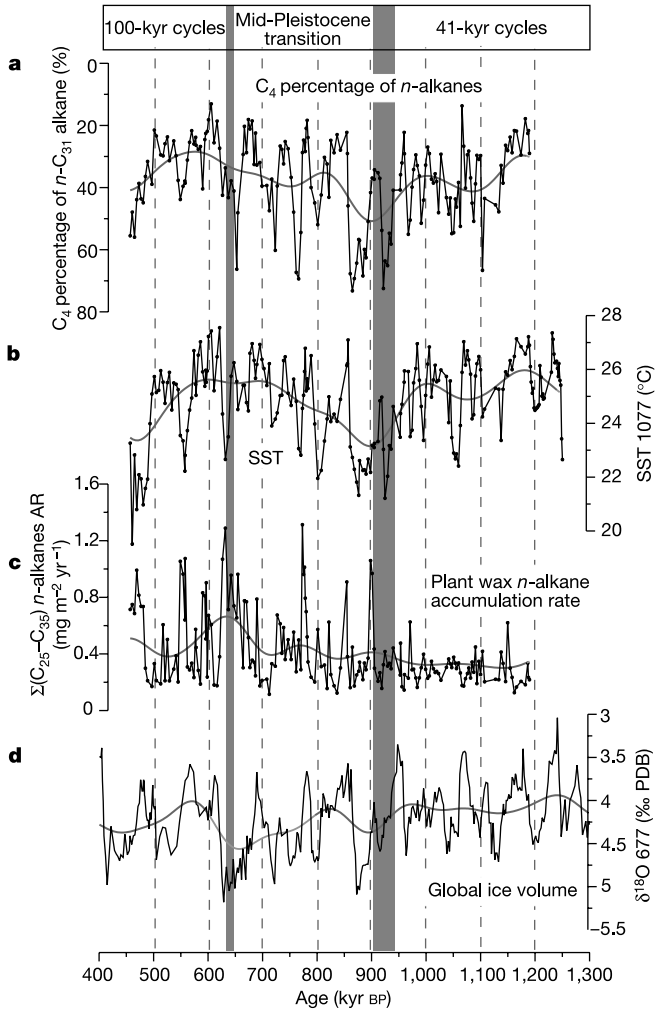

Figure 3 Mid-Pleistocene changes of African vegetation, tropical Atlantic SST, eolian plant wax transport and global ice volume. Mid-Pleistocene records of: **a**, the C_4 plant fraction of the plant wax *n*-alkanes using $\delta^{13}C$ values of the *n*-C_{31} alkane (note axis orientation); **b**, the alkenone-derived SST record at ODP Site 1077; **c**, the accumulation rates (AR) of plant-wax-derived long-chain C_{25} to C_{35} odd-numbered *n*-alkanes; and **d**, the global ice volume evolution, reflected by the oxygen isotope values of benthic foraminifera at ODP Site 677 (ref. 12) (note axis orientation). The grey lines behind the records are the long-term trends (band-pass filters with a central frequency of 0.004 (250-kyr period) and a bandwidth of 0.004 cycles per kyr). The stratigraphy of ODP Site 1077 is based on oxygen isotope analyses of *Globigerinoides ruber* (pink)[24] by correlation to the stratigraphy of ODP Site 677 (ref. 12). Ages for all samples were determined by linear interpolation using the revised composite depth scale (ref. 30). The division of the age scale into pre-MPT, transition and post-MPT indicated by the grey vertical bars is based on ref. 14.

Table 1 **Results of cross-spectral analyses**

		1/100 kyr^{-1}		1/41 kyr^{-1}		1/23 kyr^{-1}	
Data	k_0	k	Phi (°)	k	Phi (°)	k	Phi (°)
C_4 percentage	0.96	0.97	174 ± 9	0.98	−132 ± 8	0.97	−34 ± 9
SST ODP 1077	0.96	0.96	−8 ± 10	0.99	48 ± 6	0.94	−22 ± 13
ΣC_{25}–C_{35} *n*-alkanes AR	0.96	0.85	126 ± 21	0.94	144 ± 14	0.99	122 ± 4
$-\delta^{18}O$ ODP 677	0.96	0.98	24 ± 8	0.99	78 ± 5	1.00	87 ± 2

Variables are crossed with the summed orbital variance record ETP (eccentricity, tilt and precession) based on data from ref. 20. Given are the non-zero coherency at the 80% level (k_0), the coherencies (k) and phase angles (Phi) with 80% confidence intervals. Positive phase angles indicate that a variable lags the maximum interglacial forcing; negative phases indicate a lead of a variable over maximum interglacial forcing. Benthic $\delta^{18}O$ data of ODP 677 are from ref. 12. AR, accumulation rate; SST, sea surface temperature.

may thus be far more significant for large-scale environmental changes than previously thought. □

Methods

Dried and ground sediment samples were ultrasonically extracted with organic solvents. Total lipid fractions (containing the alkenones) were obtained by methylation of the extract, elution over a small silica column using ethyl acetate and silylation. Apolar fractions (containing the *n*-alkanes) were obtained by column chromatography over $AgNO_3$-impregnated, activated Al_2O_3 eluted with hexane:dichloromethane (9:1). Internal standards were added for quantification. Compounds were analysed on a Hewlett Packard 5890 series II gas chromatograph using flame ionization detection (FID) and identified by gas-chromatography mass-spectrometry analyses of selected samples. Quantification of compounds was performed by peak area integration in FID chromatograms. For SST estimation, the simplified unsaturation index ($U^{K}_{37}{}'$) was calculated from the peak areas of the di- and triunsaturated C_{37} alkenones in total lipid fractions. The conversion to SST estimates was done using: SST (°C) = $(U^{K}_{37}{}' - 0.044)/0.033$ (ref. 27). The standard deviation (±1 s.d.) based on duplicate and triplicate analyses of our samples is 0.3 °C. The compound-specific stable carbon isotopic composition of *n*-alkanes was measured through gas chromatography isotope ratio monitoring mass spectrometry using a Finnigan Delta C mass spectrometer. CO_2 gas with known isotopic composition was used as reference. Analyses were done at least in duplicate. Standard deviations of $\delta^{13}C$ values (±1 s.d.) were better than 0.5‰ against PDB.

Received 28 August 2002; accepted 18 February 2003; doi:10.1038/nature01500.

1. Collatz, G. J., Berry, J. A. & Clark, J. S. Effects of climate and atmospheric CO_2 partial pressure on the global distribution of C_4 grasses: present, past and future. *Oecologia* **114,** 441–454 (1998).
2. Pagani, M., Freeman, K. H. & Arthur, M. A. Late Miocene atmospheric CO_2 concentrations and the expansion of C_4 grasses. *Science* **285,** 876–879 (1999).
3. Huang, Y. *et al.* Climate change as the dominant control on glacial-interglacial variations in C_3 and C_4 plant abundance. *Science* **293,** 1647–1651 (2001).
4. Cerling, T. E., Wang, Y. & Quade, J. Expansion of C_4 ecosystems as an indicator of global ecological change in the late Miocene. *Nature* **361,** 344–345 (1993).
5. Kuypers, M. M. M., Pancost, R. D. & Sinninghe Damsté, J. S. A large and abrupt fall in atmospheric CO_2 concentration during Cretaceous times. *Nature* **399,** 342–345 (1999).
6. O'Leary, M. H. Carbon isotope fractionation in plants. *Phytochemistry* **20,** 553–568 (1981).
7. Cerling, T. E. *et al.* Global vegetation change through the Miocene/Pliocene boundary. *Nature* **389,** 153–158 (1997).
8. Ehleringer, J. R., Cerling, T. E. & Helliker, B. R. C_4 photosynthesis, atmospheric CO_2, and climate. *Oecologia* **112,** 285–299 (1997).
9. Eglinton, G. & Hamilton, R. J. Leaf epicuticular waxes. *Science* **156,** 1322–1335 (1967).
10. Schefuß, E., Ratmeyer, V., Stuut, J.-B. W., Jansen, J. H. F. & Sinninghe Damsté, J. S. Carbon isotope analysis of *n*-alkanes in dust from the lower atmosphere over the central eastern Atlantic. *Geochim. Cosmochim. Acta* (in the press).
11. Collister, J. W., Rieley, G., Stern, B., Eglinton, G. & Fry, B. Compound-specific $\delta^{13}C$ analyses of leaf lipids from plants with differing carbon dioxide metabolism. *Org. Geochem.* **21,** 619–627 (1994).
12. Shackleton, N. J., Berger, A. & Peltier, W. R. An alternative astronomical calibration of the lower Pleistocene timescale based on ODP Site 677. *Trans. R. Soc. Edinb. Earth Sci.* **81,** 251–261 (1990).
13. Shackleton, N. J. & Opdyke, N. O. Oxygen-isotope and paleomagnetic stratigraphy of Pacific core V28-239 late Pliocene to latest Pleistocene. *Geol. Soc. Am.* **145,** 449–464 (1976).
14. Mudelsee, M. & Schulz, M. The Mid-Pleistocene climate transition: onset of 100 ka cycle lags ice volume build-up by 280 ka. *Earth Planet. Sci. Lett.* **151,** 117–123 (1997).
15. Raymo, M. E., Oppo, D. W. & Curry, W. The mid-Pleistocene climate transition: A deep sea carbon isotopic perspective. *Paleoceanography* **12,** 546–559 (1997).
16. deMenocal, P. B. Plio-Pleistocene African climate. *Science* **270,** 53–59 (1995).
17. Wyputta, U. & Grieger, B. Comparison of eastern Atlantic atmospheric trajectories for present day and last glacial maximum. *Palaeogeogr. Palaeoclimatol. Palaeoecol.* **146,** 53–66 (1999).
18. Prell, W. L. & Kutzbach, J. E. Monsoon variability over the past 150,000 years. *J. Geophys. Res.* **92,** 8411–8425 (1987).
19. McIntyre, A., Ruddiman, W. F., Karlin, K. & Mix, A. C. Surface water response of the equatorial Atlantic Ocean to orbital forcing. *Paleoceanography* **4,** 19–55 (1989).
20. Berger, A. & Loutre, M. F. Insolation values for the climate of the last 10 million years. *Quat. Sci. Rev.* **10,** 297–317 (1991).
21. Partridge, T. C., deMenocal, P. B., Lorentz, S. A., Paiker, M. J. & Vogel, J. C. Orbital forcing of climate over South Africa: A 200,000-year rainfall record from the Pretoria saltpan. *Quat. Sci. Rev.* **16,** 1125–1133 (1997).
22. Philander, S. G. H. & Pacanowski, R. C. A model of the seasonal cycle in the tropical Atlantic Ocean. *J. Geophys. Res.* **91,** 14192–14206 (1986).
23. Katz, E. J. & Garzoli, S. L. Response of the western equatorial Atlantic Ocean to an annual wind cycle. *J. Mar. Res.* **40,** 307–327 (1982).
24. Dupont, L. M., Donner, B., Schneider, R. R. & Wefer, G. Mid-Pleistocene environmental change in tropical Africa began as early as 1.05 Ma. *Geology* **29,** 195–198 (2001).
25. Ganopolski, A., Rahmstorf, S., Petoukhov, V. & Claussen, M. Simulation of modern and glacial climates with a coupled global model of intermediate complexity. *Nature* **391,** 351–356 (1998).
26. Fontaine, B. & Bigot, S. West African rainfall deficits and sea surface temperature. *Int. J. Climatol.* **13,** 271–285 (1993).
27. Schneider, R. R., Müller, P. J. & Ruhland, G. Late Quaternary surface circulation in the east equatorial South Atlantic: Evidence from alkenone sea surface temperatures. *Paleoceanography* **10,** 197–219 (1995).
28. Sage, R. F. Environmental and evolutionary preconditions for the origin and diversification of the C_4 photosynthetic syndrome. *Plant Biol.* **3,** 202–213 (2001).
29. Petit, J. R. *et al.* Climate and atmospheric history of the past 420,000 years from the Vostok ice core, Antarctica. *Nature* **399,** 429–436 (1999).
30. Jansen, J. H. F. & Dupont, L. M. in *Proceedings of the Ocean Drilling Program, Scientific Results* Vol. 175 (ed. Wefer, G. *et al.*) (Ocean Drilling Program, College Station, Texas, 2001).

Acknowledgements We thank the Ocean Drilling Program for providing samples. The investigations were supported by the Research Council for Earth and Life Sciences with financial aid from the Netherlands Organisation for Scientific Research.

Competing interests statement The authors declare that they have no competing financial interests.

Correspondence and requests for materials should be addressed to E.S. (e-mail: schefuss@uni-bremen.de).

Fossil evidence for an ancient divergence of lorises and galagos

Erik R. Seiffert*, Elwyn L. Simons* & Yousry Attia†

* *Department of Biological Anthropology and Anatomy, Duke University, and Division of Fossil Primates, Duke Primate Center, 1013 Broad Street, Durham, North Carolina 27705, USA*
† *Egyptian Geological Museum, Misr el Kadima, Ethar el Nabi, Cairo, Egypt*

Morphological, molecular, and biogeographic data bearing on early primate evolution suggest that the clade containing extant (or 'crown') strepsirrhine primates (lemurs, lorises and galagos) arose in Afro-Arabia during the early Palaeogene[1], but over a century of palaeontological exploration on that landmass has failed to uncover any conclusive support for that hypothesis[2]. Here we describe the first demonstrable crown strepsirrhines from the Afro-Arabian Palaeogene—a galagid and a possible lorisid from the late middle Eocene of Egypt, the latter of which provides the earliest fossil evidence for the distinctive strepsirrhine toothcomb. These discoveries approximately double the previous temporal range of undoubted lorisiforms and lend the first strong palaeontological support to the hypothesis of an ancient Afro-Arabian origin for crown Strepsirrhini and an Eocene divergence of extant lorisiform families[1,3].

The primate clade Strepsirrhini—now represented by the distinctive 'toothcombed' prosimians of the Old World tropics and Madagascar—is one of the three major extant primate groups alongside Anthropoidea (monkeys, apes and humans) and Tarsiiformes (tarsiers). Within Strepsirrhini, it is clear that a major dichotomy exists between a monophyletic Lorisiformes (containing African galagos or 'bushbabies' and African and Asian lorises) and a monophyletic (and wholly Malagasy) Lemuriformes[1,4–6], but a poor strepsirrhine fossil record has left the age and place of origin of their common ancestor open to debate[7,8]. Given the probable paraphyly of African lorisiforms with respect to Asian lorises[1,3,6], the proximity of Madagascar to the African mainland[9], and the distribution of more generalized primates in the Palaeogene fossil record of northern continents and Africa[10], it is now generally believed that extant strepsirrhines shared a common Afro-Arabian ancestor[1,3], but the earliest undoubted record of crown Strepsirrhini has long been that of early Miocene (about 20 Myr old) lorisids (lorises) and galagids (galagos) from east Africa[11,12]. These Miocene lorisiforms considerably postdate estimates of basal strepsirrhine divergence times that have been reconstructed using local molecular clocks, which suggest a divergence of lorisiforms and lemuriforms 50–62 Myr ago, and a much wider window of 23–55 Myr for the divergence of lorisids and galagids[1,3,6].

Palaeontological work in 2001 led to the recovery of two Palaeogene lorisiforms from a single fossil locality, Birket Qarun Locality 2 (BQ-2), that is situated 183 m below the contact of the Qasr el Sagha and Jebel Qatrani formations north of Birket Qarun in the Fayum Depression, Egypt. This horizon was recently placed in the lowermost (Umm Rigl) Member of the Qasr el Sagha Formation[13], but